Superstripes and quasicrystals in bosonic systems with hard-soft corona interactions

Bruno R. de Abreu [1], Fabio Cinti [2,3,4] and Tommaso Macrì [1]

[1] *Departamento de Física Teórica e Experimental, Universidade Federal do Rio Grande do Norte, and International Institute of Physics, Natal-RN, Brazil*

[2] *Dipartimento di Fisica e Astronomia, Università di Firenze, I-50019 Sesto Fiorentino (FI), Italy*

[3] *INFN, Sezione di Firenze, I-50019 Sesto Fiorentino (FI), Italy*

[4] *Department of Physics, University of Johannesburg, P.O. Box 524, Auckland Park 2006, South Africa*

(Received 23 September 2020; accepted 4 March 2022; published 15 March 2022)

The search for spontaneous pattern formation in equilibrium phases with genuine quantum properties is a leading direction of current research. In this paper, we investigate the effect of quantum fluctuations—zero-point motion and exchange interactions—on the phases of an ensemble of bosonic particles with isotropic hard-soft corona interactions. We perform extensive path-integral Monte Carlo simulations to determine their ground-state properties. A rich phase diagram, parametrized by the density of particles and the interaction strength of the soft-corona potential, reveals supersolid stripes, kagome, and triangular crystals in the low-density regime. In the high-density limit, we observe patterns with 12-fold rotational symmetry compatible with periodic approximants of quasicrystalline phases. We characterize these quantum phases by computing the superfluid density and the bond-orientational order parameter. Finally, we highlight the qualitative and quantitative differences of our findings with the classical equilibrium phases for the same parameter regimes.

DOI: 10.1103/PhysRevB.105.094505

I. INTRODUCTION

The emergence of self-organized patterns from an initially disordered phase is a central subject of investigation in several branches of physics, both in the classical and in the quantum regime [1–7]. Different physical processes, both in and out of equilibrium, may display a spontaneous formation of structures described by appropriate symmetries, order parameters, or topological indices.

A central direction of research is the investigation of complex correlated phases arising from tunable two-body interaction potentials. Long-range interactions decaying as a power law with variable exponents and signs [8] are a natural framework for probing quantum droplets [9–14], stripe phases [15], hexatic or smectic crystalline phases, and recently even supersolids [16–18]. Theoretical proposals demonstrated the possibility of observing quasicrystal patterns in BECs [19,20]. Importantly, recent experiments realized two-dimensional (2D) quasicrystalline lattices [21,22], paving the way to Bose glass phases [23–25]. Likewise, finite-range potentials with single or multiple intrinsic length scales became relevant due to their experimental implementation in cavities [26], Rydberg-dressed atoms [27,28], ultra-long-range Rydberg molecules [29–32], and spin-orbit coupled Bose-Einstein condensates [33]. A common phenomenon in such systems is clustering [34–37], which results from the joint effect of a two-body interaction regular at the origin and sufficiently high densities [20,38–41]. In the opposite case of singular interparticle interactions where clustering is forbidden, one usually expects well-known (super)fluid and insulating crystalline phases. However, the effects of quantum fluctuations in systems with hard-core and multiple length-scale potentials have yet remained unexplored.

In this paper, we investigate how the zero-point motion affects the phases of 2D bosonic systems in the presence of paradigmatic microscopic hard-soft corona interactions in the zero-temperature limit. We highlight the differences with the classical equilibrium phases mapping the quantum phase diagram for a wide range of densities and interactions. We analyze the (anisotropic) superfluid properties of the system at an intermediate value of the density between the fluid and the triangular crystal phase. In addition, upon increasing the density to the maximum packing fraction, we show that patterns with 12-fold rotational symmetry can be stabilized when setting the length scale of the interparticle interaction to specific values. Notably, we emphasize the qualitative structural, and quantitative differences of our results in the quantum system with the equilibrium phases derived from classical simulations.

II. MODEL

The Hamiltonian describing a 2D system composed of N identical bosons of mass m is

$$H = -\frac{\hbar^2}{2m}\sum_{i=1}^{N}\nabla_i^2 + \sum_{i<j}^{N} V(r_{ij}). \tag{1}$$

The circularly symmetric interparticle hard-soft corona potential has the form

$$V(r_{ij}) = \begin{cases} +\infty, & r_{ij} < \sigma_0, \\ \hbar^2\varepsilon/m\sigma_0^2, & \sigma_0 < r_{ij} < \sigma_1, \\ 0, & r_{ij} > \sigma_1. \end{cases} \tag{2}$$

In Eq. (2) r_{ij} is the radial distance between the particles located at $\mathbf{r}_i$ and $\mathbf{r}_j$, respectively. It is convenient to scale

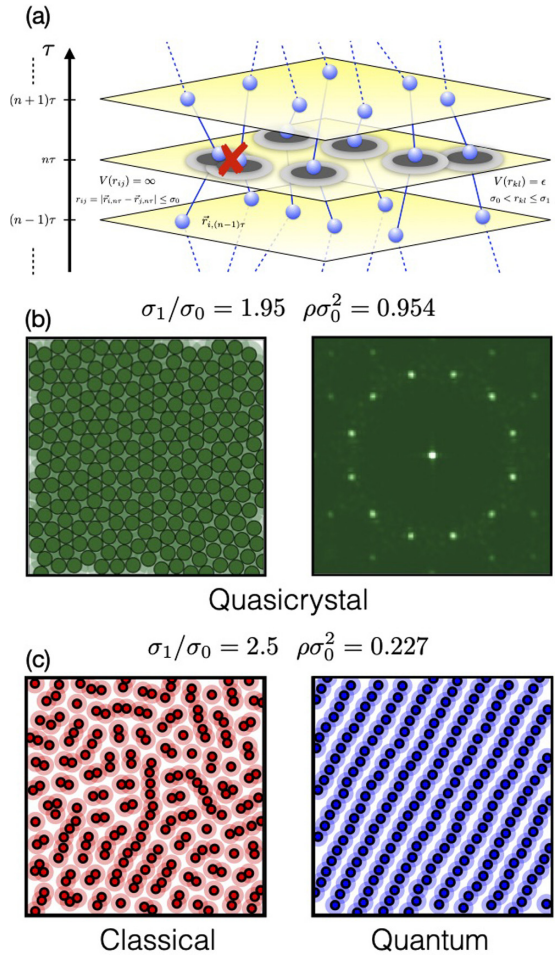

FIG. 1. (a) Representation of the worldlines of the PIMC algorithm and the constraints on the acceptance of the moves due to the hard-core interaction and the energy penalty of the soft-core potential. (b) Left: Snapshot of a metastable 12-fold quasicrystal configuration for $\sigma_1/\sigma_0 = 1.95$ and $\varepsilon = 9$ and density $\rho\sigma_0^2 = 0.954$ obtained upon initializing the simulation with a square-triangle random tiling. Centroids of the worldlines and the corresponding hard-core circle of radius σ_0 are shown. Right: Fourier transform of the 12-fold quasicrystal, where 12 main peaks are clearly visible. (c) Classical (left) and quantum (right) simulation equilibrium snapshots for the same control parameters $\sigma_1/\sigma_0 = 2.5$, $\rho\sigma_0^2 = 0.227$, and $\varepsilon = 7$. We plot the centroid and the corresponding hard-core circle. The temperature is $k_BT = 0.1\hbar^2/m\sigma_0^2$. The phase diagram of the quantum regime is discussed in Fig. 3.

lengths by the hard-core potential radius σ_0 and energies by $\hbar^2/m\sigma_0^2$. The physics of the model is then controlled by the interplay between the ratio σ_1/σ_0, the dimensionless strength of the interaction ε, and the scaled particle density $\rho\sigma_0^2$. A schematic illustration of a path-integral Monte Carlo (PIMC) configuration of a 2D ensemble of bosons interacting via the potential $V(r)$ of Eq. (2) and propagating in a discrete imaginary time τ is shown in Fig. 1(a). τ extends over the inverse temperature interval $(0, \beta)$ where $\beta = 1/k_BT$ and the parameter $t = k_BT/(\hbar^2/m\sigma_0^2)$ is the scaled temperature. Configurations in the 2D plane where the interparticle distance is smaller than the diameter of the hard-core are not allowed. When the soft coronas overlap ($\sigma_0 < r_{ij} < \sigma_1$), the configuration suffers an energy penalty ε, otherwise the interaction vanishes.

The quantum phases of this model are well known in the two limiting cases in which either σ_0 or σ_1 vanishes. In the latter case one recovers the hard-disk interaction potential, for which a liquid-solid transition takes place at $\rho\sigma_0^2 \approx 0.32$ [42]. At finite temperatures, the melting transition in two-dimensional crystals proceeds in two steps mediated by a hexatic phase [43], which is predicted to survive down to very low temperatures [44,45].

The soft-disk potential, in which σ_0 is absent, displays an even richer physics in the quantum regime [41,46]. Indeed, pair potentials with a negative Fourier component favor the formation of particle clusters, which can, in turn, crystallize to form a so-called cluster crystal. At high particle densities, well described by mean-field calculations, one finds modulated superfluid states with broken translational symmetry in the form of density waves [47]. Most interestingly, at low densities one observes the emergence of defect-induced supersolid phases in the vicinity of commensurate solid phases, as conjectured by Andreev, Lifschitz [48], and Chester [49].

III. METHODS

We carried out PIMC simulations to determine the equilibrium properties of Hamiltonian (1), hence attaining its exact ground state in the limit $T \to 0$. Simulations have been performed in the canonical ensemble with the number of particles N in the range 100–400. We employ the worm algorithm in continuous space to access genuine quantum macroscopic observables such as the superfluid fraction [50–52].

An essential ingredient of the PIMC algorithm is the estimate of the many-body density matrix at high temperature. To accurately account for the hard-soft corona interaction we first perform a pair-product approximation and then separate the contribution of the hard core and the soft core of the interaction in Eq. (2) into the *pair action*

$$u_p[\rho(\mathbf{r}, \mathbf{r}', \beta)] = -\log\left(\frac{\rho(\mathbf{r}, \mathbf{r}', \beta)}{\rho_0(\mathbf{r}, \mathbf{r}', \beta)}\right) = u_p^{\mathrm{HC}} + u_p^{\mathrm{SC}}. \quad (3)$$

In Eq. (3), $\rho(\mathbf{r}, \mathbf{r}', \beta)$ is the pair-density matrix in the center-of-mass frame interacting through Eq. (2), and $\rho_0(\mathbf{r}, \mathbf{r}', \beta)$ is the density matrix for noninteracting particles. Here, $\mathbf{r}$ ($\mathbf{r}'$) is the relative position of the pair of particles before (after) the evolution in imaginary time. The exact numerical calculation of the full pair-density matrix, while possible in principle, suffers from the strong oscillatory behavior of high angular momentum partial waves. We overcome this issue by evaluating u_p^{HC} via the well-known Cao-Berne equation for the hard-core potential in two dimensions [53,54]. Then, we calculate the contribution u_p^{SC} of the soft-corona interaction semiclassically within a WKB approach (see Supplemental Material [55] for the details of the implementation of the algorithm, including Refs. [56–67] therein).

The results in the quantum regime are compared in Fig. 1(c) with the classical equilibrium phases. The latter are obtained by employing a Monte Carlo algorithm based on classical *annealing* methods [67]. In several cases we observe distinct phases in the two regimes, confirming the relevance of quantum fluctuations at low temperatures.

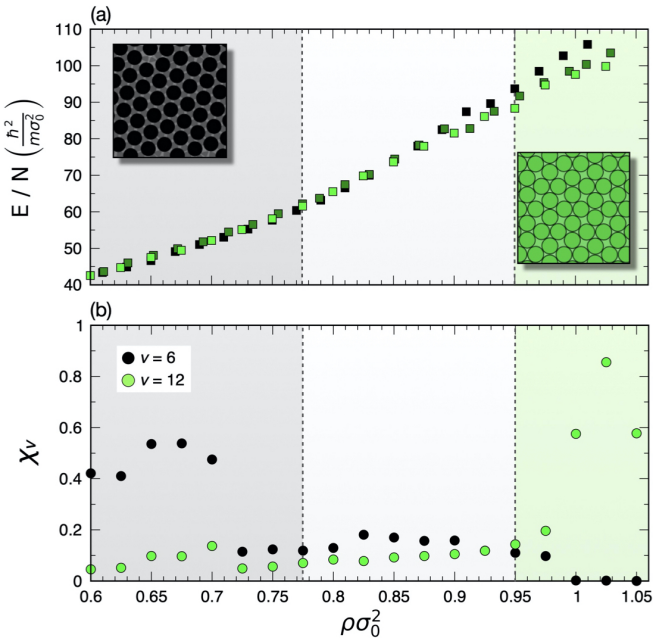

FIG. 2. High-density structural transition for an ensemble of boltzmannons interacting via the potential in Eq. (2) with $\varepsilon = 9$ when initializing the system from a triangular (black), SQRT (dark green), and a sigma phase (light green). (a) Energy per particle as a function of the scaled density $\rho\sigma_0^2$ for a system of $N = 224$ (triangular), $N = 237$ (SQRT), and $N = 200$ (sigma phase) particles at temperature $T = 0.5\,\hbar^2/m\sigma_0^2$. At low density $\rho\sigma_0^2 < 0.78$ the ground state is a triangular lattice. At high density, the system is in the sigma phase, a periodic approximant of a 12-fold quasicrystalline phase. The transition between the two phases takes place around $0.78 < \rho\sigma_0^2 < 0.95$ (gray region). The dashed lines show the position of the double tangent of the Maxwell construction. Insets: Snapshots of the centroids in the the crystalline phase at $(N, \rho\sigma_0^2) = (224, 0.75)$ and in the sigma phase 3^2434 at $(N, \rho\sigma_0^2) = (200, 1.00)$. (b) BO order parameter χ_ν of the ground state computed from Eq. (4) as a function of the scaled density across the transition with $\nu = 6$ (black) and $\nu = 12$ (green).

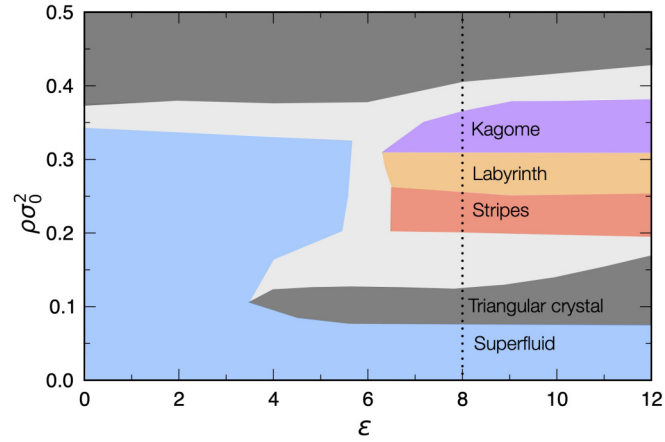

FIG. 3. Low-density ground-state phase diagram of a quantum system of $N = 200$ particles for $\sigma_1/\sigma_0 = 2.5$, $T = 0.1\hbar^2/m\sigma_0^2$ as a function of the scaled density $\rho\sigma_0^2$ and the strength of the scaled soft-corona potential ε. Superfluid (blue) and the triangular crystal (gray) at low interactions $\varepsilon \lesssim 7$, and the kagome (violet) and the triangular crystal at larger interactions. The triangular crystal phase also appears at lower densities $0.08 \lesssim \rho\sigma_0^2 \lesssim 0.19$ for $\varepsilon < 12$. At larger densities we observed a stripe phase (red), a coexistence phase (light gray), and a kagome crystal (violet). The vertical dotted line at $\varepsilon = 8$ is discussed in Fig. 4. The light gray region is a phase coexistence region.

IV. RESULTS

To investigate the emergence of nontrivial crystalline phases we examine the Fourier intensity of the density of particles $\rho(\mathbf{r}) = \sum_{i=1}^{N} \delta(\mathbf{r} - \mathbf{r}_i)$ and the pair correlation function $g(r)$ [6]. In addition, we introduce the bond-orientational order parameter (BOO) χ_ν, which accounts for the local ordering of pairs of particles,

$$\chi_\nu = \left\langle \left| \sum_{b_j} \frac{1}{N_b^{(j)}} e^{i\nu\theta_b} \right|^2 \right\rangle. \tag{4}$$

In Eq. (4) $N_b^{(i)}$ is the number of nearest-neighbor bonds of the jth particle, and θ_b is the angle between a reference axis and the bond segment. The average is performed over all particles i belonging to the same time slice $n\tau$ [see Fig. 1(a)]. We compute the respective dominant modes ν, for example, $\nu = 6$ in hexatic phases and the triangular crystal and $\nu = 12$ for a 12-fold rotational symmetry.

In Fig. 2 we discuss the high-density limit phase diagram for $\sigma_1/\sigma_0 = 1.95$ and $\varepsilon = 9$. In this regime, PIMC trajectories are only affected by zero-point motion fluctuations and it is reasonable to label those worldlines as boltzmannons rather than bosons. We refer to boltzmannons when particles are regarded as distinguishable, i.e., excluding particle exchanges [60,68,69].

Upon increasing $\rho\sigma_0^2$, we observe that a triangular lattice does not spontaneously turn into a dodecagonal quasicrystal, but a structural transition into a sigma phase is energetically favorable. It is known that a sigma phase consists of a periodic pattern that approximates the dodecagonal quasicrystalline phase [35,70]. Figure 1(b) depicts a square-triangle random tiling with prototiles given by triangles and squares (SQRT) [71] in agreement with previous classical simulations [65,66,66,72,73]. We compute the energy per particle for a wide range of densities and identify a wide coexistence region for $0.78 \lesssim \rho\,\sigma_0^2 \lesssim 0.95$ via a Maxwell double-tangent construction. We confirm our results reducing the temperature to values well below the average kinetic energy per particle. The calculation of the BOO supports our observation of the transition from a triangular lattice at low densities into a 12-fold symmetric pattern. Differently from the classical case, BOO does not saturate to unitary values due to the zero-point motion.

In Fig. 3 we show the phase diagram of the system in the limit $T \to 0$ and taking the ratio $\sigma_1/\sigma_0 = 2.5$ for a wide range of ε and intermediate densities $\rho\sigma_0^2$. For small values of ε the ground state behaves as a usual superfluid (blue region) in agreement with the properties of a liquid with pure hard-core interactions ($\varepsilon = 0$) [42,74]. Increasing the density, the system undergoes a transition from a superfluid to a

triangular crystal (gray region) around $\sigma_0^2\rho \approx 0.32$. The light gray region in between represents a coexistence phase. In the triangular crystal, the worldlines are entirely localized. For the pair interaction of Eq. (2), clustering of bosons that takes place for a pure soft-disk interaction is prohibited for parameters considered in Fig. 3.

By increasing the density $\rho\sigma_0^2$ we observe a sequence of phases breaking continuous translational symmetry into different patterns. At $\rho\sigma_0^2 \approx 0.075$ we first have a transition superfluid to solid, followed by a reentrant transition solid to superfluid. Then, at $\rho\sigma_0^2 \approx 0.2$ the system enters into a stripe phase (red). A notable feature is that this is driven entirely by quantum fluctuations. A direct comparison for $(\varepsilon, \rho\sigma_0^2) = (7.0, 0.23)$ between the classical and the quantum phases proves that the delocalization of the worldlines stabilizes the stripe configuration, whereas the corresponding classical equilibrium phase is a disordered one. The snapshot of the configuration in the classical case and the centroids of worldlines in the quantum one are respectively shown in Fig. 1(c). To corroborate this statement we computed the average kinetic energy of the stripe phase to be $E_{\rm kin}/k_BT \approx 42$, much larger than thermal fluctuations. The potential energy contributions in the two cases are instead comparable.

Within the central part of the lobe the system reorganizes into a labyrinth phase (orange) [67,75]. Upon further increasing $\rho\sigma_0^2$ the labyrinth phase is replaced by a kagome lattice (violet). Finally, for $\rho\sigma_0^2 \approx 0.35$, we encounter a phase coexistence phase region and again a triangular crystal for larger densities.

In order to fully account for the bosonic nature of the system, we include particle exchanges to calculate the superfluid fractions along the line with $\varepsilon = 8$ in Fig. 3. The superfluid fraction f_S is computed via the winding number estimator

$$f_S^{(i)} = \frac{m}{\beta\hbar^2}\frac{L_i^2}{N}\langle \hat{W}_i^2 \rangle, \tag{5}$$

where $\langle \cdots \rangle$ denotes the thermal average of the winding number operator $\hat{W}_i$ along the direction L_i with the index $i = x, y$ [76,77]. The total superfluid fraction f_S of the system is given by the trace of this tensor divided by the number of spatial dimensions of the system. The results are shown in Fig. 4 where we plot the superfluid fraction for different values of the scaled density $\rho\sigma_0^2$. Simultaneously, we extract the histogram of the permutations $P(L)$ involving L-bosons [55].

We find an insulating behavior for the triangular crystal at both low ($\rho\sigma_0^2 = 0.1$) and high densities ($\rho\sigma_0^2 = 0.45$), and the kagome crystal [Fig. 4(c)], which display vanishing superfluidity. For the latter we observe quasilocal exchanges with few particles, i.e., up to $L \approx 10$. Notably, stripes [Fig. 4(a)] display a supersolid character. Along the direction of the stripe we have $f_S^{\parallel} = 0.71(7)$, and a finite, nonzero signal, perpendicular to them, $f_S^{\perp} = 0.35(6)$. Finally, coexistence phases at intermediate densities also display a finite f_S.

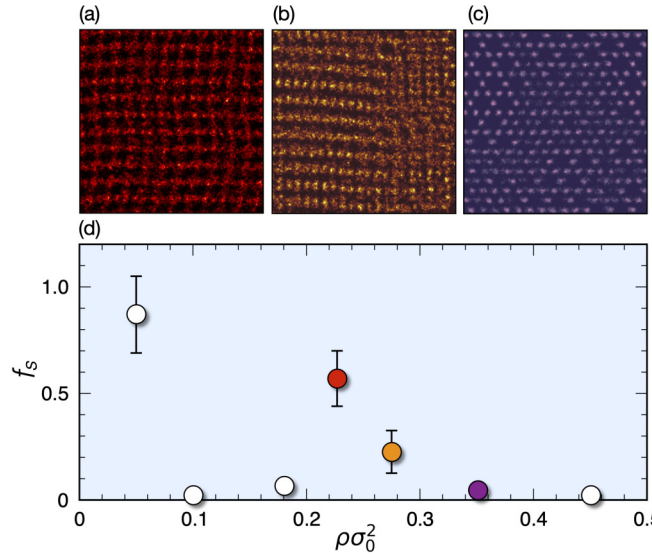

FIG. 4. Superfluidity for an ensemble of bosonic particles for $\sigma_1/\sigma_0 = 2.5$, $T = 0.1\hbar^2/m\sigma_0^2$, and $\varepsilon = 8.0$ along the vertical line of Fig. 3. (a)–(c) Snapshots of the projected worldlines. (a) Superstripe phase at $\rho\sigma_0^2 = 0.23$. (b) Phase coexistence at $\rho\sigma_0^2 = 0.275$. (c) Kagome crystal at $\rho\sigma_0^2 = 0.34$. (d) Superfluid fraction f_S as a function of scaled density $\rho\sigma_0^2$. For low density, the system is a uniform superfluid with unitary superfluidity. The triangular crystal at low ($\rho\sigma_0^2 = 0.1$) and high density ($\rho\sigma_0^2 = 0.45$) shows vanishing superfluidity. The superstripe phase at density $\rho\sigma_0^2 = 0.23$ (red circle) displays a superfluid character both along the direction of the stripes and perpendicularly to them.

V. DISCUSSION AND CONCLUSIONS

We analyzed the properties of the phases of an ensemble of bosonic particles interacting via hard-soft corona potentials in the quantum degenerate regime. We demonstrated that the phases display qualitative and quantitative differences from the classical case, especially regarding the structural properties. For instance, intricate pattern formations such as stripe phases are stabilized by quantum fluctuations and concurrently exhibit supersolid behavior. Extensions of this work include the detailed analysis of the high-density and high-interaction limit of the phase diagram to investigate the (two-step) transition from the liquid and the kagome phase to the triangular lattice [43,78]. Another interesting line concerns the study of the Berezinskii-Kosterlitz-Thouless (BKT) transition from a superfluid to normal fluid at intermediate densities both in the liquid and the stripe phase, which might be relevant for the implementation of this model in experimental platforms such as Rydberg systems, cavities, or dipolar systems [19,79–82]. The interaction potential of Eq. (2) can be implemented, e.g., via microwave shielding techniques for the hard-core barrier [30–32], combined with a dressing scheme for the soft corona whose strength can be controlled via magnetic or optical Feshbach resonances through the coupling to ultra-long-range Rydberg molecular states [29,83].

Finally, we mention that our model is studied within a pure 2D setup in the absence of external confinement along the horizontal plane. It is to be expected that the introduction of trapping along any direction (possibly anisotropic) would change qualitatively the stability of fragile patterns such as the quasicrystalline phase [84]. These results pave the ground for general classifications of interaction potentials and phases

with (quasi-)long-range orientational order, the identification of the order of phase transitions for a wide interval of densities, and interactions in the quantum regime.

ACKNOWLEDGMENTS

We thank the High-Performance Computing Center (NPAD) at UFRN as well as the Centre for High-Performance Computing (CHPC) in Cape Town for providing computational resources. B.A. acknowledges the International Institute of Physics for financial support during a visiting postdoctoral appointment. T.M. acknowledges CNPq for support through Bolsa de produtividade em Pesquisa No. 311079/2015-6. This work was supported by the Serrapilheira Institute (Grant No. Serra-1812-27802), CAPES-NUFFIC Project No. 88887.156521/2017-00.

[1] C. N. Likos, A. Lang, M. Watzlawek, and H. Löwen, Phys. Rev. E **63**, 031206 (2001).
[2] B. M. Mladek, D. Gottwald, G. Kahl, M. Neumann, and C. N. Likos, Phys. Rev. Lett. **96**, 045701 (2006).
[3] U. Gasser, E. R. Weeks, A. Schofield, P. N. Pusey, and D. A. Weitz, Science **292**, 258 (2001).
[4] P. F. Damasceno, M. Engel, and S. C. Glotzer, Science **337**, 453 (2012).
[5] X. Zeng, G. Ungar, Y. Liu, V. Percec, A. E. Dulcey, and J. K. Hobbs, Nature (London) **428**, 157 (2004).
[6] P. M. Chaikin and T. C. Lubensky, *Principles of Condensed Matter Physics* (Cambridge University Press, Cambridge, U.K., 1995).
[7] R. Shankar, *Quantum Field Theory and Condensed Matter: An Introduction* (Cambridge University Press, Cambridge, U.K., 2017).
[8] N. Defenu, T. Donner, T. Macrì, G. Pagano, S. Ruffo, and A. Trombettoni, arXiv:2109.01063.
[9] C. R. Cabrera, L. Tanzi, J. Sanz, B. Naylor, P. Thomas, P. Cheiney, and L. Tarruell, Science **359**, 301 (2018).
[10] L. Chomaz, S. Baier, D. Petter, M. J. Mark, F. Wächtler, L. Santos, and F. Ferlaino, Phys. Rev. X **6**, 041039 (2016).
[11] C. D'Errico, A. Burchianti, M. Prevedelli, L. Salasnich, F. Ancilotto, M. Modugno, F. Minardi, and C. Fort, Phys. Rev. Research **1**, 033155 (2019).
[12] I. Ferrier-Barbut, M. Schmitt, M. Wenzel, H. Kadau, and T. Pfau, J. Phys. B: At., Mol. Opt. Phys. **49**, 214004 (2016).
[13] L. Tanzi, E. Lucioni, F. Famà, J. Catani, A. Fioretti, C. Gabbanini, R. N. Bisset, L. Santos, and G. Modugno, Phys. Rev. Lett. **122**, 130405 (2019).
[14] G. Semeghini, G. Ferioli, L. Masi, C. Mazzinghi, L. Wolswijk, F. Minardi, M. Modugno, G. Modugno, M. Inguscio, and M. Fattori, Phys. Rev. Lett. **120**, 235301 (2018).
[15] J.-R. Li, J. Lee, W. Huang, S. Burchesky, B. Shteynas, F. Ç. Top, A. O. Jamison, and W. Ketterle, Nature (London) **543**, 91 (2017).
[16] M. Boninsegni and N. V. Prokof'ev, Rev. Mod. Phys. **84**, 759 (2012).
[17] J. Hertkorn, J.-N. Schmidt, M. Guo, F. Böttcher, K. S. H. Ng, S. D. Graham, P. Uerlings, T. Langen, M. Zwierlein, and T. Pfau, Phys. Rev. Research **3**, 033125 (2021).
[18] F. Böttcher, J.-N. Schmidt, J. Hertkorn, K. S. H. Ng, S. D. Graham, M. Guo, T. Langen, and T. Pfau, Rep. Prog. Phys. **84**, 012403 (2021).
[19] J. Hou, H. Hu, K. Sun, and C. Zhang, Phys. Rev. Lett. **120**, 060407 (2018).
[20] G. Pupillo, P. Ziherl, and F. Cinti, Phys. Rev. B **101**, 134522 (2020).
[21] K. Viebahn, M. Sbroscia, E. Carter, J.-C. Yu, and U. Schneider, Phys. Rev. Lett. **122**, 110404 (2019).
[22] M. Sbroscia, K. Viebahn, E. Carter, J.-C. Yu, A. Gaunt, and U. Schneider, Phys. Rev. Lett. **125**, 200604 (2020).
[23] R. Gautier, H. Yao, and L. Sanchez-Palencia, Phys. Rev. Lett. **126**, 110401 (2021).
[24] M. Ciardi, T. Macrì, and F. Cinti, Phys. Rev. A **105**, L011301 (2022).
[25] M. Ciardi, T. Macrì, and F. Cinti, Entropy **24**, 265 (2022).
[26] J. Léonard, A. Morales, P. Zupancic, T. Esslinger, and T. Donner, Nature (London) **543**, 87 (2017).
[27] J. Zeiher, R. van Bijnen, P. Schauß, S. Hild, J. yoon Choi, T. Pohl, I. Bloch, and C. Gross, Nat. Phys. **12**, 1095 (2016).
[28] V. Borish, O. Marković, J. A. Hines, S. V. Rajagopal, and M. Schleier-Smith, Phys. Rev. Lett. **124**, 063601 (2020).
[29] O. Thomas, C. Lippe, T. Eichert, and H. Ott, Nat. Commun. **9**, 2238 (2018).
[30] L. Lassablière and G. Quéméner, Phys. Rev. Lett. **121**, 163402 (2018).
[31] T. Karman and J. M. Hutson, Phys. Rev. Lett. **121**, 163401 (2018).
[32] A. V. Gorshkov, P. Rabl, G. Pupillo, A. Micheli, P. Zoller, M. D. Lukin, and H. P. Büchler, Phys. Rev. Lett. **101**, 073201 (2008).
[33] Y. J. Lin, K. Jiménez-García, and I. B. Spielman, Nature (London) **471**, 83 (2011).
[34] A. J. Archer, A. M. Rucklidge, and E. Knobloch, Phys. Rev. E **92**, 012324 (2015).
[35] K. Barkan, M. Engel, and R. Lifshitz, Phys. Rev. Lett. **113**, 098304 (2014).
[36] L. Caprini, E. Hernández-García, and C. López, Phys. Rev. E **98**, 052607 (2018).
[37] S. Gopalakrishnan, I. Martin, and E. A. Demler, Phys. Rev. Lett. **111**, 185304 (2013).
[38] N. Henkel, R. Nath, and T. Pohl, Phys. Rev. Lett. **104**, 195302 (2010).
[39] F. Cinti, P. Jain, M. Boninsegni, A. Micheli, P. Zoller, and G. Pupillo, Phys. Rev. Lett. **105**, 135301 (2010).
[40] R. Díaz-Méndez, F. Mezzacapo, W. Lechner, F. Cinti, E. Babaev, and G. Pupillo, Phys. Rev. Lett. **118**, 067001 (2017).
[41] F. Cinti, T. Macrì, W. Lechner, G. Pupillo, and T. Pohl, Nat. Commun. **5**, 3235 (2014).
[42] L. Xing, Phys. Rev. B **42**, 8426 (1990).
[43] E. P. Bernard and W. Krauth, Phys. Rev. Lett. **107**, 155704 (2011).
[44] W. Lechner, H.-P. Büchler, and P. Zoller, Phys. Rev. Lett. **112**, 255301 (2014).
[45] G. M. Bruun and D. R. Nelson, Phys. Rev. B **89**, 094112 (2014).

[46] T. Macrì, S. Saccani, and F. Cinti, J. Low Temp. Phys. **177**, 59 (2014).
[47] T. Macrì, F. Maucher, F. Cinti, and T. Pohl, Phys. Rev. A **87**, 061602(R) (2013).
[48] A. F. Andreev and I. M. Lifshitz, Sov. Phys. - JETP **29**, 1107 (1969).
[49] G. V. Chester, Phys. Rev. A **2**, 256 (1970).
[50] N. Henkel, F. Cinti, P. Jain, G. Pupillo, and T. Pohl, Phys. Rev. Lett. **108**, 265301 (2012).
[51] M. Boninsegni, N. Prokof'ev, and B. Svistunov, Phys. Rev. Lett. **96**, 070601 (2006).
[52] M. Boninsegni, N. V. Prokof'ev, and B. V. Svistunov, Phys. Rev. E **74**, 036701 (2006).
[53] E. de Prunelé, J. Phys. A: Math. Theor. **41**, 255305 (2008).
[54] S. Pilati, S. Giorgini, and N. Prokof'ev, Phys. Rev. Lett. **100**, 140405 (2008).
[55] See Supplemental Material at http://link.aps.org/supplemental/10.1103/PhysRevB.105.094505 for details on the density matrices, the bond-orientational order, temperature and initial conditions, and the differences between classical and quantum behavior.
[56] I. M. Gel'fand and A. M. Yaglom, J. Math. Phys. **1**, 48 (1960).
[57] H. F. Trotter, Proc. Am. Math. Soc. **10**, 545 (1959).
[58] N. Wiener, J. Math. Phys. **2**, 131 (1923).
[59] A. Borodin, J. Math. Sci. **99**, 1044 (2000).
[60] D. M. Ceperley, Rev. Mod. Phys. **67**, 279 (1995).
[61] R. Jastrow, Phys. Rev. **98**, 1479 (1955).
[62] V. Zampronio and S. Vitiello, Phys. Rev. B **99**, 045145 (2019).
[63] J. Barker, J. Chem. Phys. **70**, 2914 (1979).
[64] S. Pilati, Studies of ultracold gases using quantum Monte Carlo techniques, Ph.D. thesis, Universitá Degli Studi di Trento, 2000.
[65] T. Dotera, T. Oshiro, and P. Ziherl, Nature (London) **506**, 208 (2014).
[66] H. Pattabhiraman and M. Dijkstra, Soft Matter **13**, 4418 (2017).
[67] G. Malescio and G. Pellicane, Nat. Mater. **2**, 97 (2003).
[68] M. Boninsegni, L. Pollet, N. Prokof'ev, and B. Svistunov, Phys. Rev. Lett. **109**, 025302 (2012).
[69] F. Cinti, M. Boninsegni, and T. Pohl, New J. Phys. **16**, 033038 (2014).
[70] C. L. Henley, Phys. Rev. B **43**, 993 (1991).
[71] M. O'Keeffe and M. M. J. Treacy, Acta Crystallogr., Sect. A **66**, 5 (2010).
[72] M. Oxborrow and C. L. Henley, Phys. Rev. B **48**, 6966 (1993).
[73] H. Pattabhiraman, A. P. Gantapara, and M. Dijkstra, J. Chem. Phys. **143**, 164905 (2015).
[74] P. W. Leung and G. V. Chester, Phys. Rev. B **43**, 735 (1991).
[75] G. Malescio and G. Pellicane, Phys. Rev. E **70**, 021202 (2004).
[76] E. L. Pollock and D. M. Ceperley, Phys. Rev. B **36**, 8343 (1987).
[77] V. G. Rousseau, Phys. Rev. B **90**, 134503 (2014).
[78] A. L. Thorneywork, J. L. Abbott, D. G. A. L. Aarts, and R. P. A. Dullens, Phys. Rev. Lett. **118**, 158001 (2017).
[79] S. V. Rajagopal, T. Shimasaki, P. Dotti, M. Račiūnas, R. Senaratne, E. Anisimovas, A. Eckardt, and D. M. Weld, Phys. Rev. Lett. **123**, 223201 (2019).
[80] F. Mivehvar, H. Ritsch, and F. Piazza, Phys. Rev. Lett. **123**, 210604 (2019).
[81] F. Cinti and M. Boninsegni, J. Low Temp. Phys. **196**, 413 (2019).
[82] A. Safavi-Naini, B. Capogrosso-Sansone, A. Kuklov, and V. Penna, New J. Phys. **18**, 025017 (2016).
[83] N. Sándor, R. González-Férez, P. S. Julienne, and G. Pupillo, Phys. Rev. A **96**, 032719 (2017).
[84] F. Cinti and T. Macrì, Condens. Matter **4**, 93 (2019).